NASA Technical Memorandum 84393

A Laser Velocimeter System for Large-Scale Aerodynamic Testing

Michael S. Reinath, Kenneth L. Orloff, and Philip K. Snyder

January 1984

NASA
National Aeronautics and
Space Administration

NASA Technical Memorandum 84393

A Laser Velocimeter System for Large-Scale Aerodynamic Testing

Michael S. Reinath
Kenneth L. Orloff
Philip K. Snyder, Ames Research Center, Moffett Field, California

National Aeronautics and
Space Administration

Ames Research Center
Moffett Field, California 94035

SYMBOLS

B	distance between beams at output window
f	Doppler frequency measured by counter processor
f_D	offset frequency due to frequency shifting
N	number of cycles per frequency measurement
n	number of samples per velocity measurement
R	distance from output window to measuring volume
S	estimator of the standard deviation of the assumed isotropic fluctuations
S_v, S_w, S_{v_m}	estimators of the standard deviations of the V_i, W_i, V_{m_i} distributions, respectively
V, W	velocity component along Y-axis and Z-axis, respectively
V_m	directly measured velocity component
$\bar{V}_m$	directly measured velocity component mean
V_R	resultant velocity vector in Y, Z-plane
Y, Z	Cartesian coordinates
Z_c	confidence coefficient
α	tilt angle measured from vertical
β	angle between output laser beams
$\eta_{\bar{V}}, \eta_{\bar{W}}$	absolute statistical error ratio for the mean velocity V and W, respectively
λ	laser wavelength (514.5 nm)
τ	Doppler period measured by counter processor

Subscripts:

1,2	lateral positions of the velocimeter
i	index of a distribution

SUMMARY

A unique laser velocimeter has been developed that is capable of sensing two orthogonal velocity components from a variable remote distance of 2.6 to 10 m for use in the 40- by 80-Foot and 80- by 120-Foot Wind Tunnels and the Outdoor Aerodynamic Research Facility at Ames Research Center. The system hardware, positioning instrumentation, and data acquisition equipment are described in detail; system capabilities and limitations are discussed; and expressions for systematic and statistical accuracy are developed. Direct and coupled laboratory measurements taken with the system are compared with measurements taken with a laser velocimeter of higher spatial resolution, and sample data taken in the open circuit exhaust flow of a 1/50-scale model of the 80- by 120-Foot Wind Tunnel are presented.

INTRODUCTION

Mechanical probes are the customary means by which velocity is measured in large wind tunnels. Although they afford a basic and dependable method of making such measurements, mechanical probes have two significant disadvantages. First, the structure generally required for probe support is often bulky and complex, as well as costly, especially if probe translation is desired over long distances. Second, measurements made in this way can contain errors caused by interference introduced by the probe itself and the support structure in the immediate vicinity of the probe, as well as the interference and blockage caused by the remote parts of the support structure.

The laser velocimeter (LV) is far more desirable than mechanical probes for making flow-field velocity measurements in large wind tunnels because the laser system can be implemented with minimal mechanical complexity and with minimal modifications to the test-section structure. Furthermore, by incorporating a variable-focus capability, a laser velocimeter can be used for surveying large regions without introducing objectionable support structures in the immediate vicinity of the measurement location; thus, it eliminates the potential interference introduced by these structures.

A major portion of the work in the field of long-range laser velocimetry has been devoted to the development of systems designed to make atmospheric wind-velocity measurements. The early systems used CO_2 lasers in the local oscillator configuration, had relatively poor spatial resolution, and could only measure the velocity component along the beam axis. They were used, for example, to make atmospheric wind-velocity measurements (refs. 1 and 2), to study full-scale wake flows (refs. 3 and 4), and, as recently as 1980, to measure the flow around a V/STOL aircraft operating in ground effect (ref. 5). Systems in which the dual-beam backscatter technique is used with visible laser light have since been developed to improve spatial resolution — for example, those by Durst et al. (ref. 6) and Danielsson (ref. 7). These systems too are used for remote sensing of wind velocity. A system of this type but more suitable for the applications under consideration was developed by

Hancy and Koeneke (ref. 8) who used a pulsed dye laser for in-flight measurement of flow fields around aircraft and in large wind tunnels at ranges from 3.5 to 5 m.

The velocimeter described herein was designed to operate at ranges necessary for use in the 40- by 80-Foot and 80- by 120-Foot Wind Tunnel test sections, as well as in the Outdoor Aerodynamic Research Facility. Possible applications include V/STOL vehicle flow-field mapping for location and sizing of wakes and plumes, wing-loading distribution determination without the need for pressure taps, and investigations of high-lift airfoil and rotating rotor-blade aerodynamics.

SYSTEM DESCRIPTION

General

A diagram showing the laser velocimeter installed within the test section of the 40- by 80-Foot Wind Tunnel is shown in figure 1. It is a single-color, dual-beam, scanning confocal backscatter LV that directly senses two orthogonal components of velocity and indirectly obtains the third orthogonal component by a transformation of coupled velocity components.

The laser head and system optics are mounted within a streamlined cylindrical aluminum shell; the shell is 0.76 m in diameter and 4.3 m in length and is supported on bearings to permit rotation about its longitudinal axis. A faired, tubular aluminum framework, 2.7 m long, 0.61 m high, and 0.66 m wide, supports the streamlined cylinder and serves as a housing for the laser power supply, cooling system components, stepper-motor drivers, and other miscellaneous components. This framework is, in turn, mounted to a carriage assembly that attaches to a rail support system to permit lateral translation.

Optical Hardware

A high-power, argon-ion, continuous-wave laser, operated at a wavelength of 514.5 nm, is used as the source of laser light. The laser and power supply (fig. 2) are supplied with deionized cooling water from a closed-loop system through a flexible hose assembly to permit lateral scanning of the instrument. An electric pump, mounted near the laser power supply at the base of the instrument, is required to boost the water pressure to achieve the necessary flow rate of 4.8 gal/min for cooling.

The beam exits the laser and is immediately turned through an angle of 180° by two dielectrically coated mirrors before entering a quartz acousto-optic cell in which the beam is split. The cell is driven at a frequency of 110 MHz and can accept the full 9-W power of the unexpanded beam at the operating wavelength with an efficiency of approximately 50% in the first order, without perceptible distortion of the transmitted beams. The cell driver is equipped with a signal-amplitude adjustment that is normally used for optimizing the cell output, but in this case serves as a fine adjustment of the splitting operation.

The unshifted and first-order beams exit the first acousto-optic cell and enter a double-wedge prism assembly that is used to deflect the beams in the proper direction for fine adjustment. A separating prism (fig. 3) separates the beams ahead of

the second acousto-optic cell. This cell is driven at a frequency of 90 MHz and can accept the full power of the unexpanded, unshifted beam with minimal distortion and with an efficiency of 85% in the first order. A major advantage of this dual-cell system, whose function it is to resolve the directional ambiguity in addition to splitting the beam is the large frequency difference that results between the Doppler and cell-driver frequencies. Electronic noise radiated by the cell drivers does not pose a potential signal-processing problem, as it sometimes does in single-cell systems; the location of the noise on the spectrum is far from the Doppler frequency, thereby permitting its easy removal by filtering.

Double-wedge prisms are used for fine adjustment of the beam direction ahead of the rhomboid rotator assembly. By properly adjusting these wedge prisms, the beams, which have been shifted by 90 and 110 MHz, respectively, can be forced to emerge from the rhomboid rotator parallel and with a spacing of 5.0 cm.

The rhomboid rotator assembly has two distinct positions, as shown in figure 4. In the unrotated position, the beams pass through the assembly undisturbed, remaining in the horizontal plane. In the rotated position, however, the beams enter the rhomboid prisms in the horizontal plane, experience two total internal reflections, and emerge with the same spacing in the vertical plane. A final set of double-wedge prisms is attached to the rotating assembly to provide a means of resetting the parallelism of the beams in this plane.

The lens system designed for use in the 40- by 80-Foot Wind Tunnel is composed of three lens modules and operates nearly at the diffraction limit over the intended focus range — a minimum distance of 2.6 m to a maximum of 10 m from the output lens. Over this range, the measuring volume increases in length (fig. 5) and is appoximately 0.025 cm in diameter at mid-range. The output module is a stationary singlet that has a clear aperture diameter of 33 cm. The intermediate module is also a stationary singlet, and the module that first intercepts the parallel beams is a movable triplet assembly. The folding mirror, which is 51 cm long, 38 cm wide, and 6.4 cm thick, is dielectrically coated for 99.94% reflectance at the operating wavelength and an incidence angle of 45°.

The lens system functions as the receiving as well as the transmitting system. Scattered light follows the path taken by the transmitted light on its return through the lens system and is ultimately reflected by a pair of metallic mirrors and focused by a small positive lens into an adjustable pinhole located on the face of the phototube housing (see fig. 2). Light that enters the pinhole passes through an interference filter before it enters the phototube.

Extension to Longer Range

The insert in figure 2 shows a set of interchangeable lenses that extend the focus range of the LV to 10 to 20 m for use in the 80- by 120-Foot Wind Tunnel and at the Outdoor Aerodynamic Research Facility. Instead of using the transmitting system itself for collecting scattered light, a separate, coaxial, multi-element receiving lens module is used to improve noise immunity. This module remains stationary while the photomultiplier assembly is translated so as to maintain focus of the image at various ranges. Its position is determined by the controller interface which is programmed to position the assembly relative to the focusing element of the transmission system.

Preliminary testing of this configuration has yet to be conducted to determine the performance and the type of signal processing necessary.

Positioning Hardware

In order to perform flow surveys in a plane perpendicular to the longitudinal axis of the velocimeter, the test-point location can be moved by rotating the upper cylindrical portion of the instrument about its longitudinal axis, translating the entire unit laterally, and optically focusing from within the instrument (see fig. 1); a change in the longitudinal location of the survey plane is accomplished by translation of the rail system, which is only temporarily attached to the wind-tunnel floor. Rotation of the instrument about its longitudinal axis positions the test point at any location along an arc that extends 45° to either side of the vertical or the horizontal (depending on how the detachable folding-mirror/output-window assembly is installed) with a possible resolution limit of 0.20 mrad. Translation of the instrument on the 6-m-long rails positions the test point laterally with a minimum resolution of 0.025 cm, and optical focusing controls the range with a nominal resolution of 0.11 cm. These motions are provided by three computer-controlled stepper motors; positions are monitored by absolute, 15-bit, optical shaft-angle encoders.

The angular scan is performed by a stepper motor operating in the half-step mode, 400 steps per revolution to provide maximum resolution. The cylindrical shell is driven by the motor through a low backlash 120-to-1 gear reducer. The associated one-turn, 15-bit encoder turns with the instrument through an angular displacement that cannot exceed one-quarter turn.

The stepper motor that performs the lateral scan has a resolution of 200 steps per revolution and is connected to the instrument through a 50-to-1 gear reducer and a rack-and-pinion drive assembly. The associated 64-turn, 15-bit encoder is also driven with a rack-and-pinion drive assembly modified to have zero backlash.

The remaining stepper motor controls the focus range; it operates in the half-step mode to provide maximum resolution for positioning the movable lens module that is mounted on a precision translation stage. The stage is driven by a lead screw that has a pitch of 10 threads per inch and is attached directly to the stepper motor. The associated 64-turn, 15-bit encoder is belt-driven at a 1-to-1 gear ratio by the motor.

Data-Acquisition and Positioning Instrumentation

A dedicated, stand-alone, microprocessor-based controller/interface unit, especially designed for use with this velocimeter system, is used to acquire and buffer data, control motor motion, and monitor encoder positions. The unit, shown in the system schematic of figure 6, can acquire data generated by a maximum of three counter processors and is capable of acquiring peripheral data on 10 analog and 4 digital channels.

The controller/interface unit can be configured to conditionally sample the counter processor data by using one or more the the 4 digital channels and up to 4 of the 10 analog channels as conditional signals. In this mode of operation, maximum and minimum allowable signal levels are selected on the front panel of the

unit for each analog or digital channel on which the conditional sampling is to depend. Whenever the signal in any of the selected channels falls outside the preset signal level limits, the LV processors are inhibited, thereby halting the flow of data to the controller/interface buffer.

The controller/interface unit communicates with a microprocessor located in the velocimeter instrument through a 20-mA current loop (see fig. 5). This microprocessor directly controls motor motion and monitors encoder positions and the associated limit switches. When motor motion is requested, the on-board microprocessor picks the largest possible predetermined high, low, or base motor speed that can be used to move the incremental length of the requested move and insures that the correct encoder position is reached. It also handles the problem of mechanical backlash by insuring that any requested encoder position is approached consistently from the same direction.

The controller/interface unit can be operated manually (local control) from the front panel where position and velocity are displayed continuously in user units. Alternatively, it may be operated remotely through an IEEE-488 interface bus by either a desk-top computer with dual flexible-disk mass storage or a high-speed mainframe minicomputer system with graphics capability. In the remote mode of operation, the interrupt feature of the IEEE-488 interface is employed to optimize data acquisition and reduction. This feature frees the computer, after a command has been transferred to the controller/interface, and enables it to perform other tasks, such as data reduction, during the period of time required to execute the requested operation. The controller/interface regains the attention of the computer by asserting an interrupt when it is ready for the next instruction. A status word can be requested by the computer to confirm the cause of the interrupt, for example, position reached, data buffer ready for transfer, or data acquisition complete.

MEASUREMENT PROCEDURE

General

The optical system of the velocimeter focuses the source laser beams at a particular location in the velocity field. The coherent, monochromatic laser light produces interference fringes at this location that are perpendicular to the plane formed by the beams themselves. A particle moving with the flow field through the measuring volume scatters light as it traverses each bright fringe. A small portion of the scattered light is collected by the lens system and is focused at the photomultiplier tube, generating a signal that oscillates at the fringe-crossing rate of the particle. The period of this oscillation is measured by the counter processor and represents the time taken by the particle to move the perpendicular distance between the fringes. Since the fringe spacing is a known quantity, the velocity component perpendicular to the fringes is easily obtained by division of the spacing by the period.

The two acousto-optic cells, driven at frequencies of 90 and 110 MHz, resolve the problem of directional ambiguity by generating interference fringes that move rather than remain stationary. A 20-MHz Doppler signal, the beam-pair frequency difference, is generated when stationary particles are present in the measuring volume. Excursions about this frequency, produced by particles traversing the measuring volume, indicate not only the magnitude of the velocity component but also its direction.

Velocity-Component Measurement

The orthogonal components of velocity sensed directly by the velocimeter are depicted in figure 7. The component measured by the unrotated beam-pair is oriented in a direction perpendicular to the longitudinal axis of the instrument. When the rhomboid beam rotator is actuated, either remotely through software control or manually at the controller/interface, the beam-pair assumes the orientation shown in figure 7(b) and senses the component parallel to the longitudinal axis; approximately 1 sec is required to perform the beam rotation.

The third orthogonal component of velocity is not directly sensed by the instrument, but can be obtained (fig. 8) by making measurements at a given point in the flow field from two different lateral positions of the instrument. The desired orthogonal components of velocity, V and W, oriented with respect to the primary coordinate system, are calculated using the transformation equations

$$V = \frac{V_{m_1} \sin \alpha_2 - V_{m_2} \sin \alpha_1}{\sin(\alpha_2 - \alpha_1)}$$

$$W = \frac{V_{m_1} \cos \alpha_2 - V_{m_2} \cos \alpha_1}{\sin(\alpha_2 - \alpha_1)}$$

with

$$V_{m_1} = \frac{\lambda(f_1 - f_D)}{2 \sin \beta_1/2}$$

$$V_{m_2} = \frac{\lambda(f_2 - f_D)}{2 \sin \beta_2/2}$$

where V_{m_1} and V_{m_2} are the velocities directly sensed by the LV; $\lambda = 514.5$ nm; f_D is the 20-MHz offset frequency produced by the acousto-optic cells; f_1 and f_2 are the frequencies of the burst signals measured by the counter processors; and the angles α_1, α_2, β_1, and β_2 are defined in figure 8.

System Calibration

Two types of calibrations are necessary to position accurately the velocimeter probe volume with respect to the reference coordinate system, and to obtain velocity measurements once it is in position. The first calibration type is needed to relate encoder counts to user coordinates, and the second is required to convert measured frequency to velocity.

The calibrations required for lateral positioning along the rails and tilt positioning about the longitudinal axis are linear with position and are relatively easy to obtain. Moreover, the calibrations remain unchanged unless the gear mechanisms that drive the respective encoders are modified; therefore, they need not be repeated for various velocimeter applications. In contrast, the range calibration that relates zoom position to encoder counts is nonlinear and requires a third-order

polynomial curve fit. Furthermore, a new calibration must be acquired each time it becomes necessary to significantly realign the beams to correct for drift.

The calibration required to convert the frequency measured by the counter processor to velocity is also nonlinear and is fitted with a third-order polynomial as a function of range. It is normally performed concurrently with the calibration for zoom position and is subject to the same condition that realignment of the beams requires recalibration.

SYSTEM ACCURACY

Systematic Uncertainty Analysis

The relative systematic uncertainty present in a directly measured velocity component, designated V_m, is the nonrandom error that consistently influences all measurements equally and can be expressed primarily in terms of the relative uncertainties present in the measured parameters f, R, and B, as

$$\frac{\Delta V_m}{V_m} = \frac{\Delta f}{f} + \cos^2 \beta \, \frac{\Delta R}{R} + (1 + \sin^2 \beta) \, \frac{\Delta B}{B} \tag{1}$$

where the first term on the right-hand side of equation (1) represents the relative systematic uncertainty present in the Doppler frequency measurement made by the counter processor, and the remaining two terms represent the systematic uncertainty contribution owing to the configuration geometry.

The first term in equation (1) can be written in terms of other parameters as

$$\frac{\Delta f}{f} = \frac{\Delta \tau \lambda f^2}{2NV_m \sin \beta/2}$$

where $\Delta\tau$ is the resolution of the counter-processor clock and N is the number of cycles chosen for processing.

A parametric study was performed to determine the relative contribution of each of the terms in equation (1) to the final systematic uncertainty, $\Delta V_m/V_m$. The term $\Delta f/f$ was found to dominate the expression at lower measurement velocities such as those most likely to occur in the Y,Z-plane of figure 8 during a typical wind-tunnel-type application. The relative contribution of $\Delta f/f$ to the total uncertainty $\Delta V_m/V_m$ is shown in figure 9 as a function of V_m for various values of N at a range of 6.4 m and at a Doppler frequency of 20 MHz. For example, at a velocity of V_m = 20 m/sec, the term $\Delta f/f$ constitutes approximately 85% of the total systematic uncertainty present in the velocity measurement V_m. The second and third terms in equation (1) are, therefore, negligible relative to the frequency term at lower measurement velocities, and equation (1) reduces to

$$\Delta V_m = \frac{\Delta \tau \lambda f^2}{2N \sin \beta/2}$$

The systematic uncertainty present in the V- and W-components of figure 8 can be expressed in terms of the systematic uncertainty present in both the V_m measurement and the measured geometrical parameters. Several terms expressing uncertainty caused by geometry are negligible, and the resulting expressions reduce to

$$\frac{\Delta V}{\Delta V_m} = \frac{|\sin \alpha_1| + |\sin \alpha_2|}{|\sin(\alpha_2 - \alpha_1)|}$$

$$\frac{\Delta W}{\Delta V_m} = \frac{|\cos \alpha_1| + |\cos \alpha_2|}{|\sin(\alpha_2 - \alpha_1)|}$$

where the ratios $\Delta V/\Delta V_m$ and $\Delta W/\Delta V_m$ represent the number of times that the minimum systematic uncertainty is increased when it becomes necessary to determine a velocity component indirectly from coupled measurements rather than measuring it directly.

Figure 10 shows how the V-component uncertainty ratio, $\Delta V/\Delta V_m$, varies with coupling angle $(\alpha_2 - \alpha_1)$ and mean tilt angles $(\alpha_1 + \alpha_2)/2)$. Notice that very little additional uncertainty is incurred at any coupling angle by measuring the V-component indirectly if the beam pairs are oriented on opposite sides of the vertical (i.e., when the coupling angle is chosen to be greater than twice the mean tilt angle). The corresponding family of curves for the W-component uncertainty ratio, $\Delta W/\Delta V_m$, are shown in figure 11. Notice that coupling angle has a substantial effect on the uncertainty ratio for the wind-tunnel application shown in figure 8 because the mean tilt angle cannot exceed 45° in this configuration; hence, a maximum coupling angle must be maintained to minimize systematic uncertainty for this configuration.

At a measurement velocity V_m of 100 m/sec, for example, a direct measurement can be made at mid-range with a systematic uncertainty of ±1.5%, from equation (1), when 16 cycles are chosen for processing. An indirect measurement, on the other hand, made at a coupling angle of 60° and a mean tilt angle of 0°, for example, will yield two orthogonal velocity components, V and W, as shown in figure 8, with systematic uncertainties larger than the corresponding direct measurements. The systematic uncertainty of the V-component will be 1.2 times as large (see fig. 10) and the W-component will be 1.9 times as large (see fig. 11). Greater accuracy can be obtained, however, by increasing the number of cycles chosen for processing or by operating the counter processor in the total-burst mode so that all the cycles of the burst are included in the frequency measurement.

Statistical Uncertainty Analysis

If variations owing to signal processing particle lag, biasing, and systematic uncertainty are negligible, deviations of the instantaneous velocity measurement from the true mean velocity are primarily attributable to the statistically time-dependent fluctuations of the flow field. Estimators of the true mean velocity and true standard deviation about the directly measured mean component of velocity are given by the ensemble average,

$$\bar{V}_m = \frac{1}{n} \sum_{i=1}^{n} V_{m_i}$$

and

$$S_{V_m} = \left(\frac{1}{n-1} \sum_{i=1}^{n} \left(V_{m_i} - \bar{V}_m \right)^2 \right)^{1/2}$$

respectively. Furthermore, the confidence interval for the directly measured mean velocity component is given (ref. 9) by

$$\Delta V_m = \pm \frac{Z_c S_{V_m}}{\sqrt{n}} \tag{2}$$

where Z_c is the confidence coefficient corresponding to a particular confidence level (e.g., $Z_c = 1.96$ for a confidence level of 95%).

The estimators of the standard deviations about the indirectly measured velocity components V and W can be obtained from the estimators of the standard deviations about the directly measured components V_{m_1} and V_{m_2}, using the method described in reference 10. When events from channels 1 and 2 are uncorrelated, as for nonsimultaneous measurements, the resulting expressions reduce to

$$S_V^2 = \frac{1}{\sin^2(\alpha_2 - \alpha_1)} \left(\sin^2 \alpha_2 \, S_{V_{m_1}}^2 + \sin^2 \alpha_1 \, S_{V_{m_2}}^2 \right)$$

$$S_W^2 = \frac{1}{\sin^2(\alpha_2 - \alpha_1)} \left(\cos^2 \alpha_2 \, S_{V_{m_1}}^2 + \cos^2 \alpha_1 \, S_{V_{m_2}}^2 \right)$$

If fluctuations within the flow are assumed to be isotropic, the expressions reduce further to

$$\eta_{\bar{V}} = \left(\frac{\sin^2 \alpha_2 + \sin^2 \alpha_1}{\sin^2(\alpha_2 - \alpha_1)} \right)^{1/2}$$

$$\eta_{\bar{W}} = \left(\frac{\cos^2 \alpha_2 + \cos^2 \alpha_1}{\sin^2(\alpha_2 - \alpha_1)} \right)^{1/2}$$

where $\eta_{\bar{V}}$ and $\eta_{\bar{W}}$ represent the number of times that the absolute statistical error in the respective components increases because of the coordinate transformation. The absolute statistical error in each of the respective components becomes

$$\Delta V = \pm \frac{Z_c S}{\sqrt{n}} \eta_{\bar{V}} \tag{3}$$

and

$$\Delta W = \pm \frac{Z_c S}{\sqrt{n}} \eta_{\bar{W}} \tag{4}$$

where S is an estimator of the isotropic fluctuations.

Figure 12 presents the variation of $\eta_{\bar{V}}$ with coupling angle at various mean tilt angles. The absolute uncertainty ratio approaches infinity as the coupling angle approaches zero, and it approaches unity as the coupling angle approaches 90°. Furthermore, the ratio increases with mean tilt angle. The ratio has a minimum value of $1/\sqrt{2}$ at zero coupling angle and zero mean tilt angle, because each beam pair directly measures the V-component in this case, doubling the effective number of samples taken. The curves of the W-component ratio are identical in shape (fig. 13). Notice, however, that the respective mean tilt angles of the corresponding curves in figures 12 and 13 are complementary angles.

For the wind-tunnel-type configuration of figure 8, maximum statistical accuracy is achieved for the V-component of velocity at zero mean tilt angle and zero coupling angle. Conversely, when obtaining the W-component of velocity, maximum accuracy is achieved at maximum coupling angle and maximum mean tilt angle, for the same configuration. As an example, consider a flow with an isotropic free-stream turbulence intensity of 5%. One can be 95% confident that any measured velocity component V_m has a statistical mean-velocity accuracy of better than ±1% with 100 samples, using equation (2). Furthermore, when making indirect measurements, for example, at a coupling angle of 30° and a mean tilt angle of 20°, the statistical accuracy for the mean V-component measurement can be expected to be ±1.2%, using equation (3) and figure 12, with the same number of samples and confidence level. Similarly, the statistical accuracy for the mean W-component measurement can be expected to be ±2.5%, using equation (4) and figure 13, also with the same conditions.

SAMPLE MEASUREMENTS

To evaluate system performance in a laboratory environment, the flow field generated by a four-bladed, 0.76-in.-diam, industrial-type air-circulation fan was studied parallel to the plane of rotation on the downstream side. Several surveys were made at a distance of 0.56 fan diameters from the blades through the axis of symmetry. The surveys, shown in figure 14, were made while introducing a light mineral-oil aerosol upstream of the fan to increase the data rate. Acceptable data were also obtained when only natural seeding was present in the flow, although at a much lower rate. Each data point represents the average of 100 velocity samples taken at a laser output power of 3 W, using 16 Doppler cycles for processing. A 95% conference interval is shown with each point.

To study the worst-case spatial resolution, surveys were made with the probe volume oriented along the survey direction so that the axial and tangential velocity components were measured directly. The figure shows results obtained at ranges of 3.1 and 8.4 m from the center of the fan. A survey was also made using the two-dimensional portion of a smaller scale three-dimensional laser velocimeter (ref. 11) that has a much higher spatial resolution (1.5 mm); the data obtained are plotted in figure 14(b) for comparison. The agreement is encouraging, especially when the

highly turbulent nature of the flow is considered. The only significant disagreement occurs in the shear region at the center of the tangential profile where the effects of poorer spatial resolution are apparent. Based on the shear measured by the three-dimensional LV, the velocity variation across the probe volume of the long-range LV is estimated to be 4 m/sec when operating at the 8.4-m range; as a result, the long-range LV could not be expected to fully resolve the correct shear.

Figure 14(a) also shows a survey that was generated from indirect measurements made at nominal coupling and mean tilt angles of 40° and 0°, respectively. According to figure 13, the statistical uncertainty increases by a factor of about 2 at these angles for a coupled measurement of the W-component, the component indirectly measured in this case. The associated 95% confidence intervals in the figure are, therefore, of the order of twice those corresponding to the directly measured components of figure 14(b); hence, the agreement is quite good throughout the survey, since most of the confidence intervals overlap. Moreover, the velocity shear resolved at the center of the profile by the indirect measurements almost equals that resolved the the three-dimensional LV, because the probe volume remained almost perpendicular to the survey direction throughout the survey, and the spatial resolution was determined by the diameter rather than the length of the probe volume.

An application of the system to the measurement of another flow is shown in figure 15. Vertical surveys were made through the exhaust flow generated by a 1/50-scale model of the 80- by 120-Foot Open-Circuit Wind Tunnel. The objectives were to determine the velocities present in the exhaust flow from the exit to a full-scale altitude of 900 ft in order to determine the size and shape of the exhaust flow, and to test various deflector-ramp configurations so that the parameters important in minimizing the flow velocity near the ground could be determined.

The surveys shown in the figure were performed with the velocimeter positioned at a particular fixed downstream location through a combination of tilting and focusing, and required about 50 min each to complete. One hundred velocity samples were acquired per measurement over a focus range that extended from a minimum of 4.5 m to a maximum of 8.4 m.

Scatter in the vector direction is most apparent in the survey taken 5.5 m from the tunnel exit; it is believed that these variations are due to the influence of ambient air currents; the currents were minimized, but could not be completely eliminated. Again, a light mineral-oil aerosol was introduced at the tunnel inlet to increase the data rate, although excellent signals were obtained with natural seeding — a data rate of about 30 particles/sec was obtained with seeding as opposed to about 1 particle/sec with natural seeding.

A direct measurement of the vertical and horizontal velocity components was made at each location along each survey line using the beam-rotation feature provided by the rhomboid rotator assembly. A sample vertical survey, the survey taken 1.8 m from the tunnel exit, is shown in figure 16. Each vertical component was obtained by making a small cosine correction to the tilted measurement (it was verified that no significant lateral flow was present in the survey plane). Horizontal surveys were also made, but are not shown.

CONCLUSION

A laser-velocimeter system was developed and tested which can operate over the extended ranges necessary to make aerodynamic measurements around large-scale models such as those tested in the 40- by 80- and 80- by 120-Foot Wind Tunnels at Ames Research Center. Its feasibility as a practical flow-measurement device was demonstrated by making detailed, nonintrusive velocity surveys in the exhaust flow of a 1/50-scale model of the 80- by 120-Foot Wind Tunnel. No elaborate survey probe-support structures were required, setup time for preparing the velocimeter was minimal, and the surveys were made over relatively short periods of time.

Systematic and statistical accuracies were investigated for both direct and coupled velocity measurements and the important parameters affecting accuracy were identified. Generalized equations were developed that predict the system accuracy; they will be used in future applications.

The feasibility of making accurate and practical coupled velocity measurements was demonstrated in the laboratory environment, and the system spatial resolution was compared with that of an LV with much higher spatial resolution.

REFERENCES

1. Lawrence, T. R.; Wilson, D. J.; et al.: A Laser Velocimeter for Remote Wind Sensing. Rev. Sci. Instrum., vol. 43, Mar. 1972, pp. 512-517.

2. Hughes, A. J.; and Pike, E. R.: Remote Measurement of Wind Speed by Laser Doppler Systems. Appl. Opt., vol. 12, no. 3, Mar. 1973, pp. 597-601.

3. Wilson, D. J.; Zalag, A. D., et al.: Full-Scale Wake Flow Measurements with a Mobile Laser Doppler Velocimeter. J. Aircraft, vol. 16, no. 3, Mar. 1979, pp. 155-161.

4. Huffaker, R. M.; Jelalian, A. V.; and Thomson, A. L.: Laser-Doppler System for Detection of Aircraft Trailing Vortices. Proceedings of the IEEE, vol. 58, no. 3, Mar. 1970, pp. 322-326.

5. Zalag, A. D.; Brashears, M. R.; Jordan, A. J.; Shrider, K. R.; and Vought, C. D.: Measurement of Flow around V/STOL Aircraft with an LDV System. J. Aircraft, vol. 17, no. 12, Dec. 1980, pp. 835-836.

6. Durst, F.; Howe, B.; and Richter, G.: LDA-System Design for Long-Range Wind-Velocity Measurements. Proceedings of the Symposium on Long Range and Short Range Optical Velocity Measurements, German-French Research Institute, R117/80, Sept. 1980, pp. XI-1 to XI-9.

7. Danielsson, L.: Laser Doppler Velocity Measurements over Large Distances in the Atmosphere. Proceedings of the Symposium on Long Range and Short Range Optical Velocity Measurements, German-French Research Institute, R117/80, Sept. 1980, pp. XII-1 to XII-11.

8. Hancy, J. P.; and Koeneke, A.: Compact Fringe-Type Anemometer for Airborne and Large Wind Tunnel Applications. Proceedings of the Symposium on Long Range and Short Range Optical Velocity Measurements, German-French Research Institute, R117/80, Sept. 1980, pp. X-1 to X-8.

9. Spiegel, M. R.: Probability and Statistics. McGraw-Hill, New York, 1975.

10. Orloff, K. L.; and Snyder, P. K.: Laser Doppler Anemometer Measurements Using Nonorthogonal Velocity Components: Error Estimates. Appl. Opt., vol. 21, Jan. 1982, pp. 339-344.

11. Snyder, P. K.; Orloff, K. L.; and Aoyagi, K.: Performance and Analysis of a Three-Dimensional Nonorthogonal Laser Doppler Anemometer. NASA TM-81283, 1981.

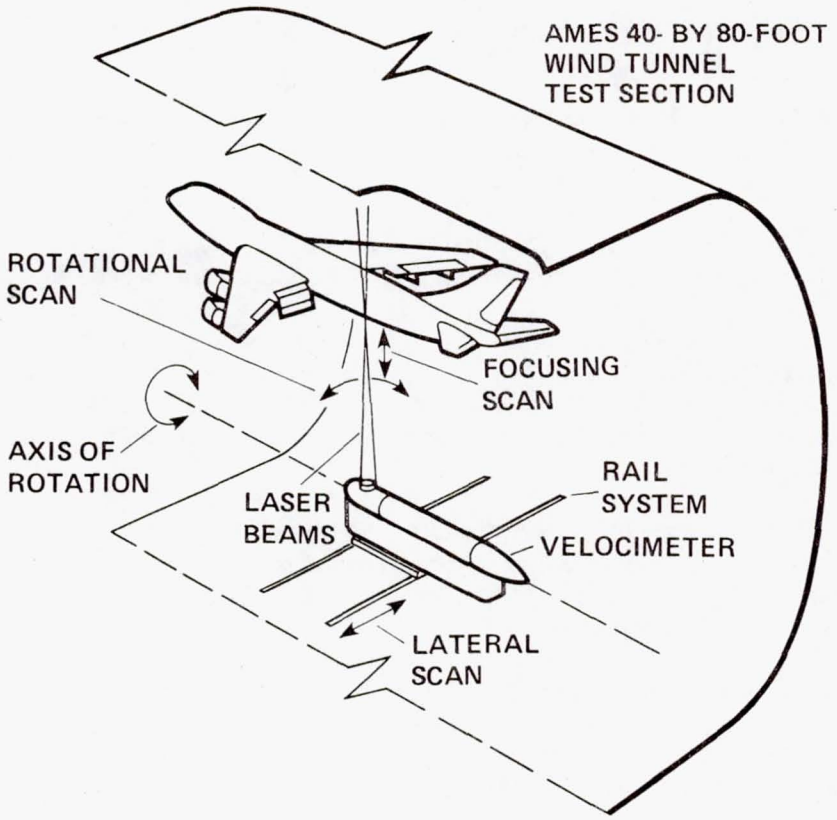

Figure 1.- Wind-tunnel application of the velocimeter showing degrees of test-point positioning freedom.

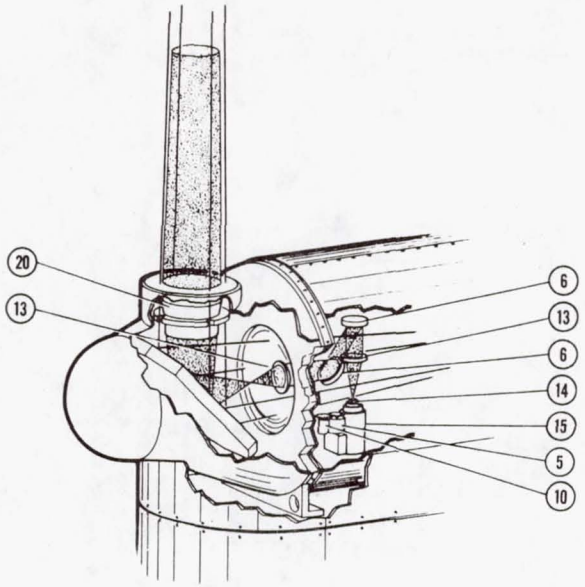

1 FOLDING MIRROR
2 OUTPUT LENS
3 INTERMEDIATE LENS
4 TRANSLATING LENS MODULE
5 FOCUSING STEPPER MOTOR
6 MIRROR
7 RHOMBOID ROTATOR ASSEMBLY
8 BEAM-SPLITTER AND FREQUENCY-SHIFTER
9 LASER
10 ABSOLUTE ENCODER
11 GEAR REDUCER
12 ANGLE-ROTATION STEPPER MOTOR
13 FOCUSING LENS
14 PINHOLE AND INTERFERENCE FILTER
15 PHOTOMULTIPLIER TUBE
16 LASER POWER SUPPLY
17 LINEAR BEARING
18 TRANSLATION STAGE
19 LATERAL TRANSLATION STEPPER MOTOR
20 RECEIVING LENS

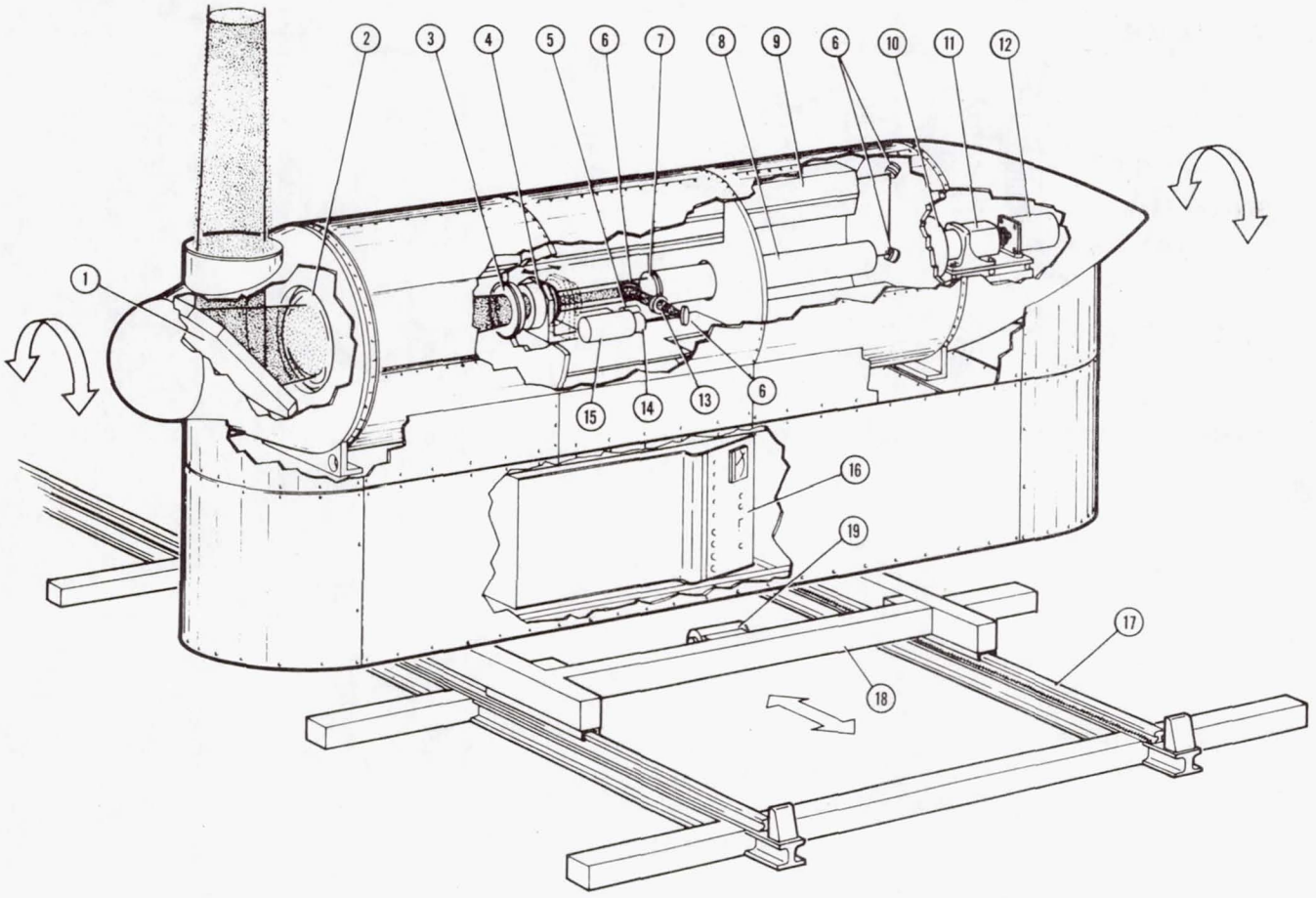

Figure 2.- Laser velocimeter system shown mounted on lateral traversing rails; insert shows alternative method of receiving for extended-range configuration (both beam pairs are shown in the insert).

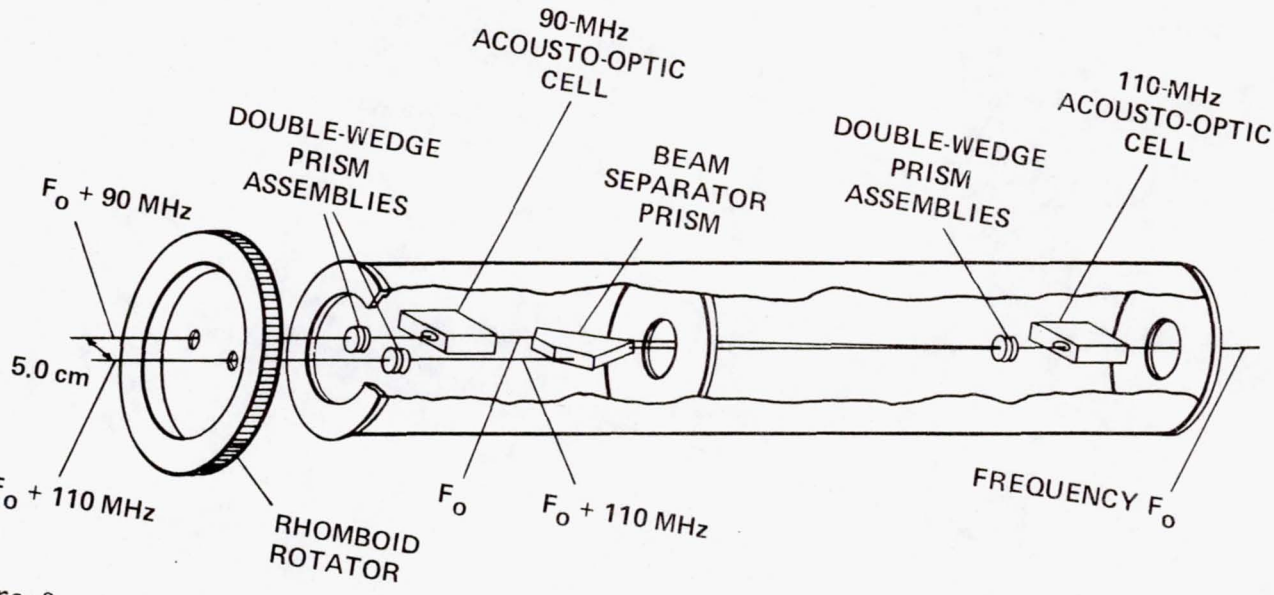

Figure 3.- Beam-splitter/frequency-shifter assembly (rhomboid rotator shown without prisms).

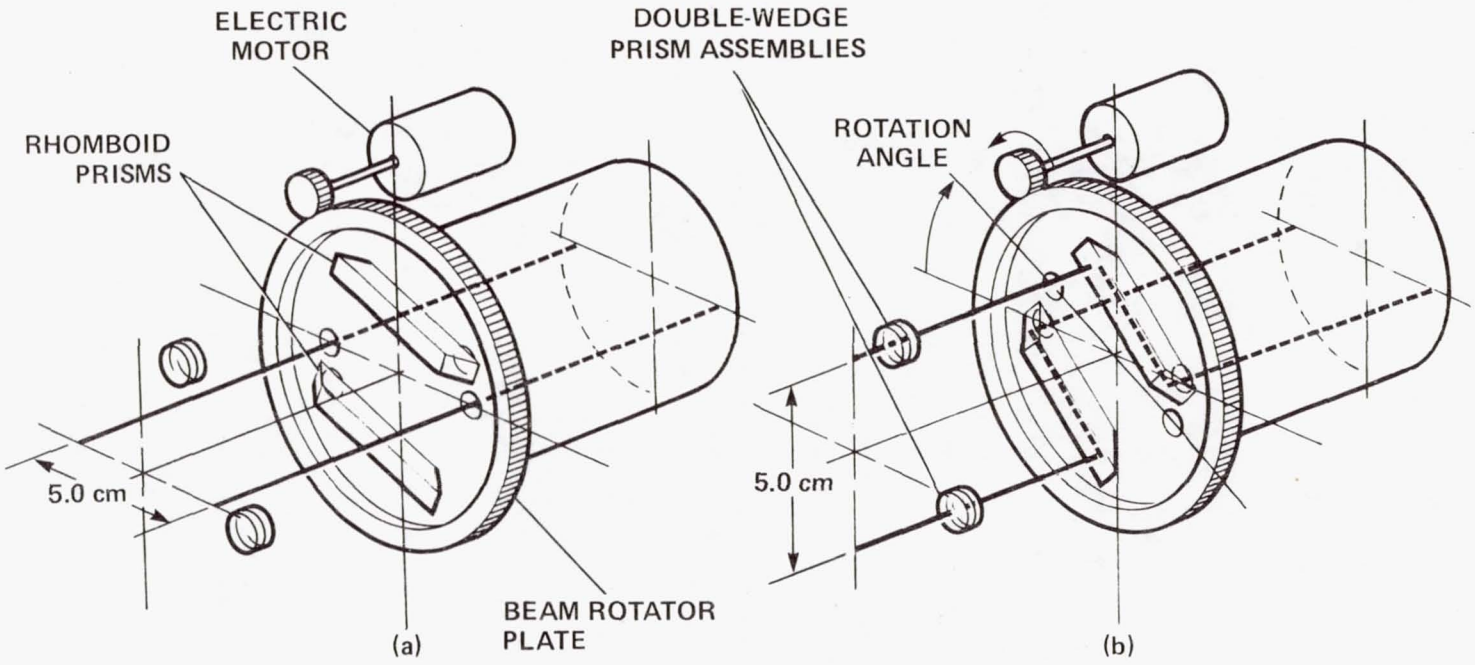

Figure 4.- Rhomboid rotator assembly shown in the: (a) unrotated position; (b) rotated position.

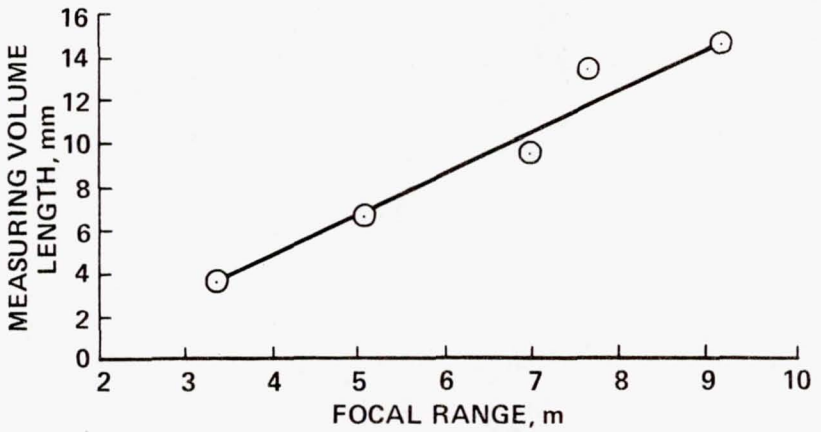

Figure 5.- Measuring-volume length measured between $1/e^2$ intensity points shown as a function of range.

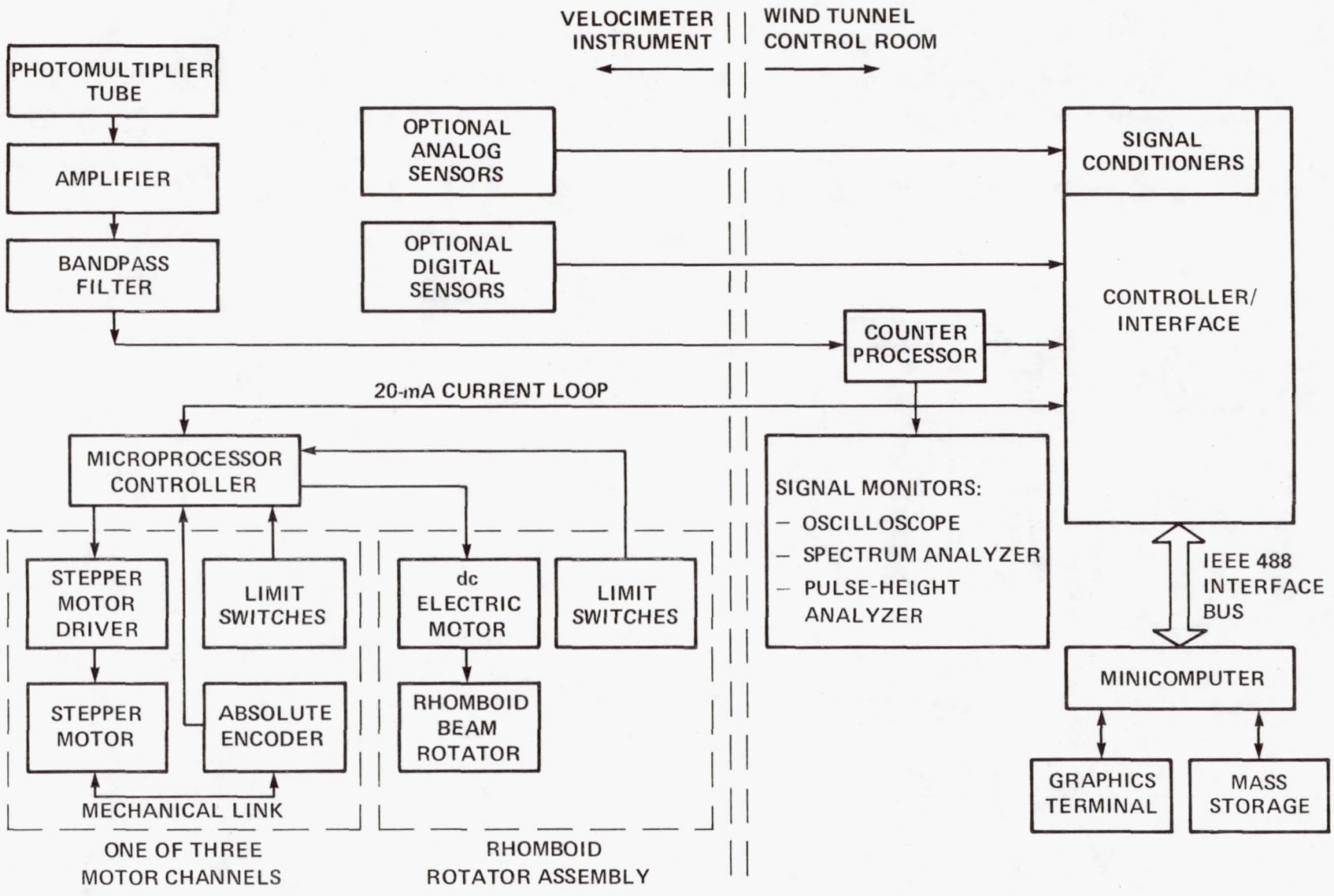

Figure 6.- System schematic showing equipment for management of data acquisition and positioning.

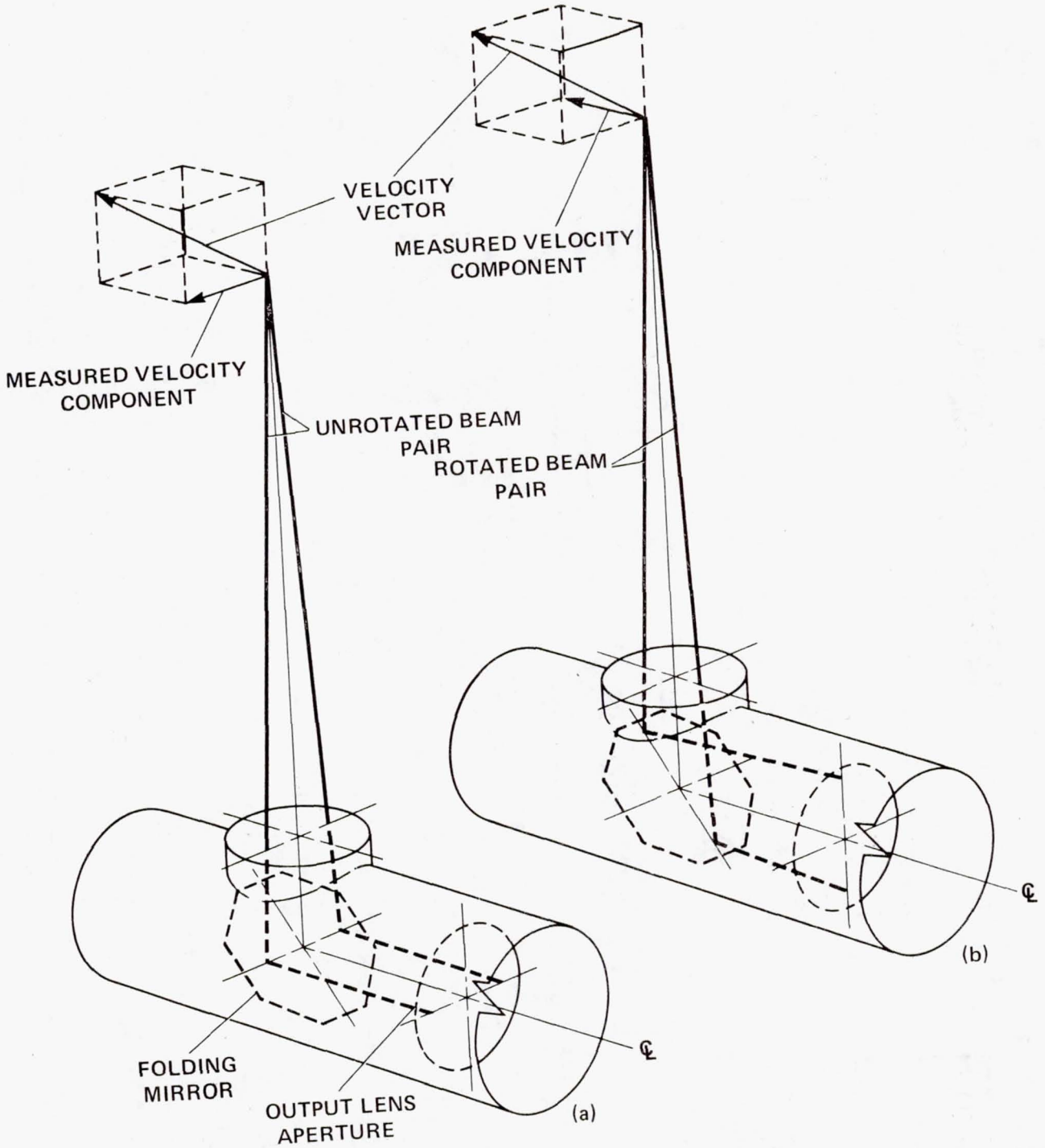

Figure 7.- Velocimeter output window assembly showing the orientation of velocity components measured by: (a) unrotated beam pair; (b) rotated beam pair.

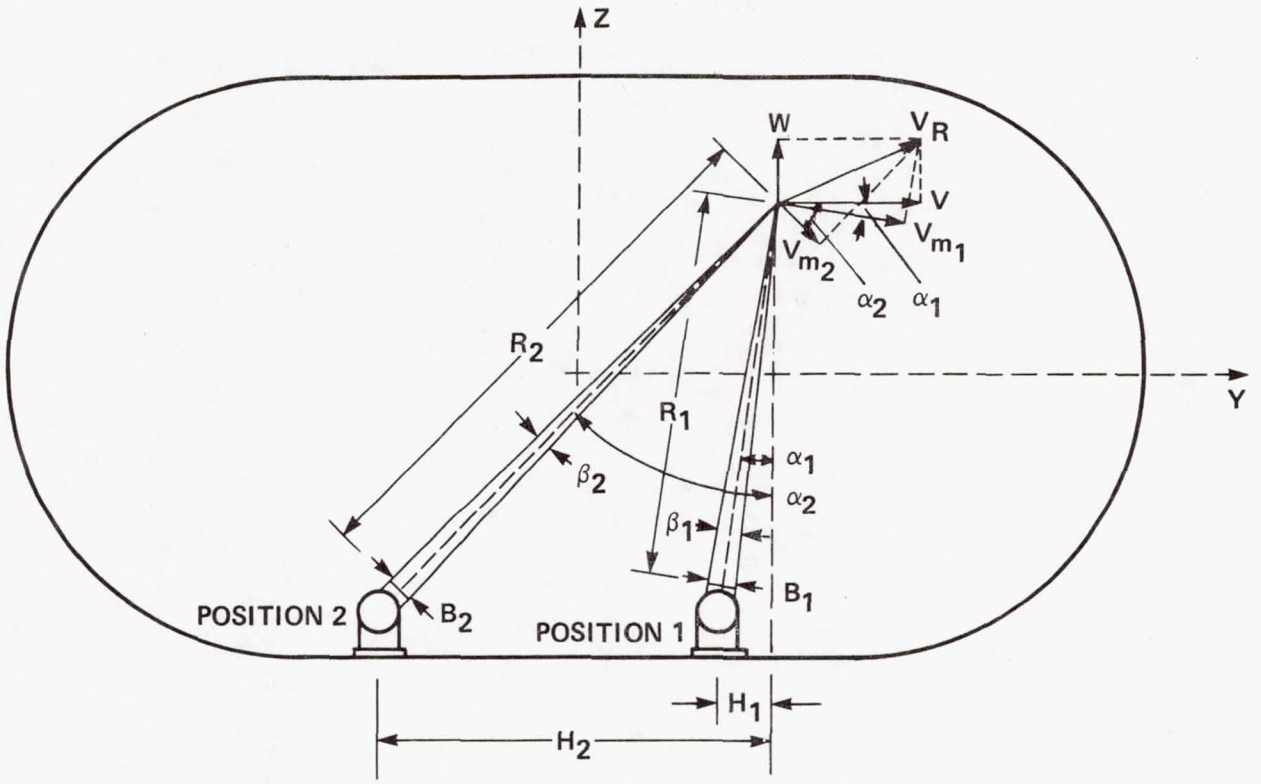

Figure 8.- Method and nomenclature for obtaining orthogonal velocity components from nonorthogonal measurements shown for a typical wind-tunnel application (V_R is the resultant velocity vector in the Y,Z-plane, and V_{m_1} and V_{m_2} are the directly measured components).

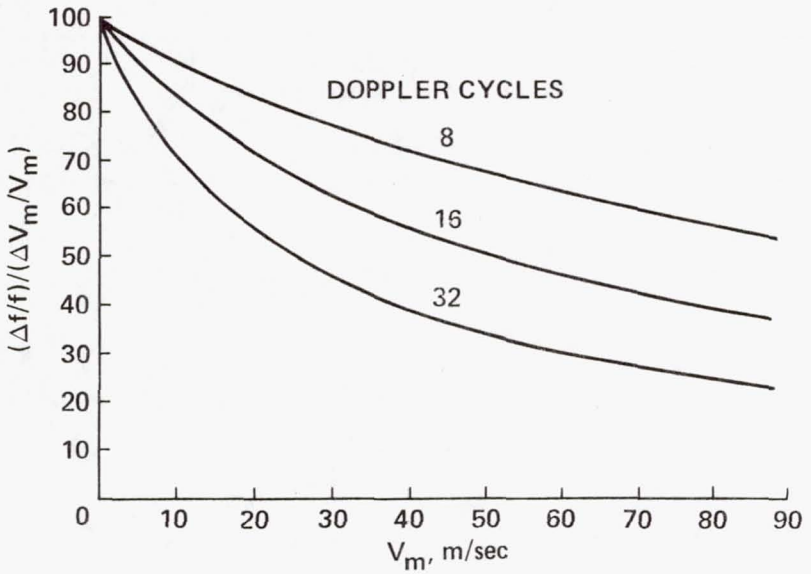

Figure 9.- Relative contribution of the frequency term $\Delta f/f$ in equation (5) to the final uncertainty $\Delta V_m/V_m$ for various numbers of Doppler cycles chosen for processing (range = 6.4 m, $\Delta\tau$ = 2 nsec, Doppler frequency nominally 20 MHz).

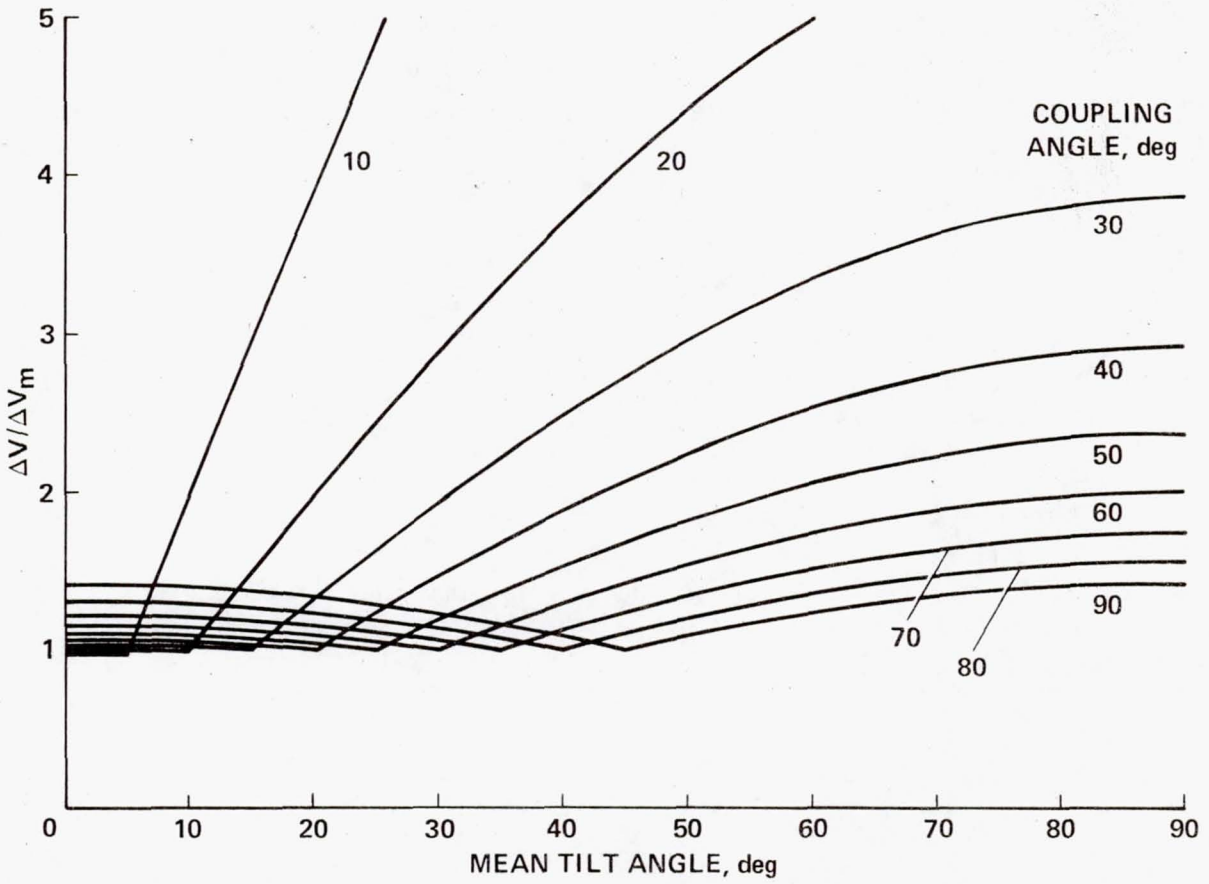

Figure 10.- Absolute systematic uncertainty ratio for the V-component of velocity.

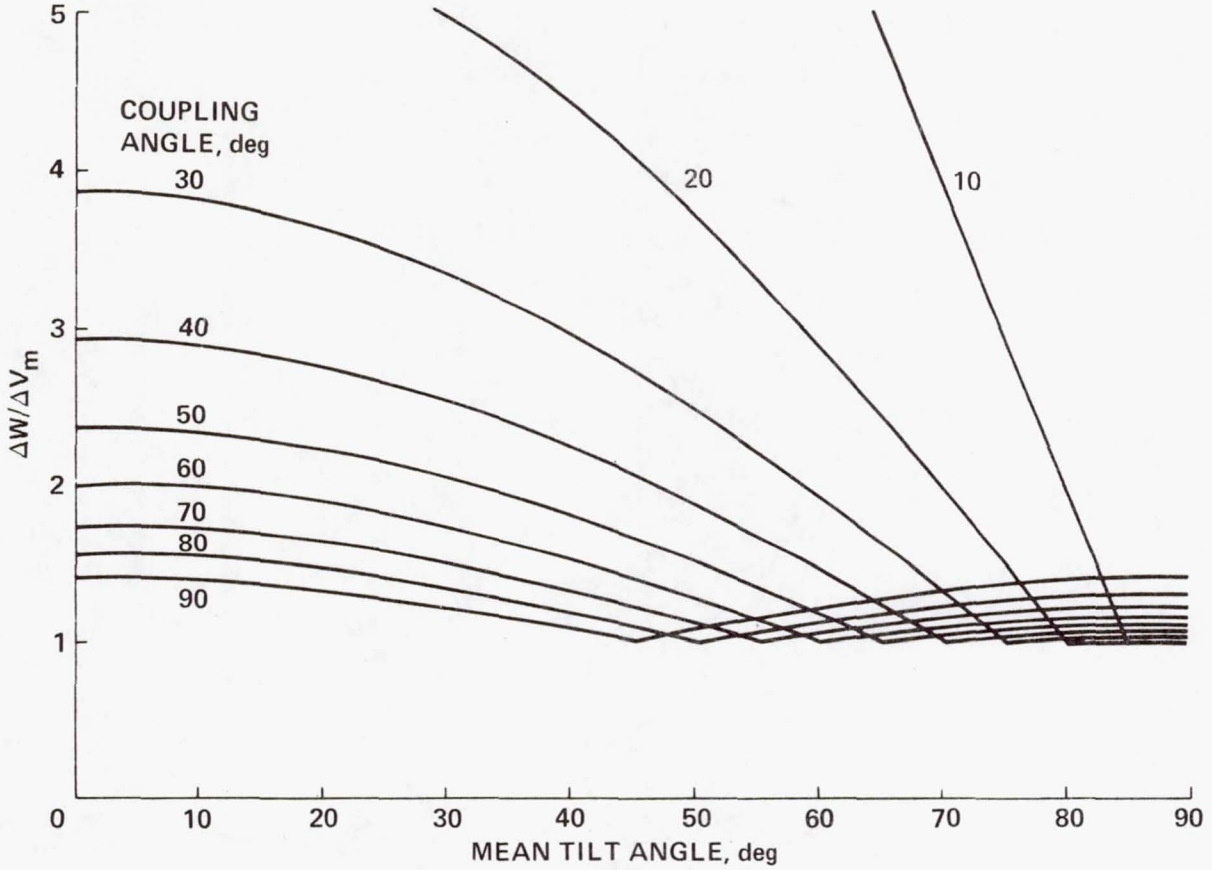

Figure 11.- Absolute systematic uncertainty ratio for the W-component of velocity.

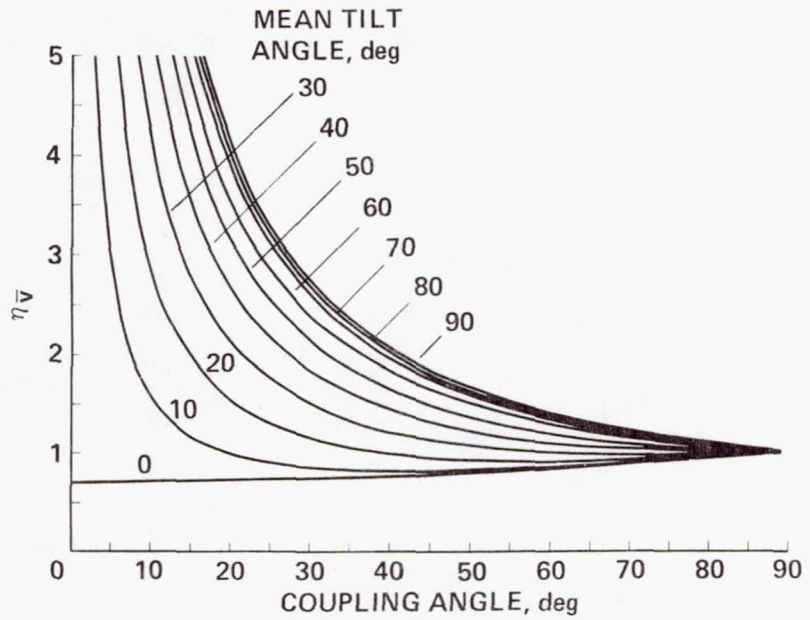

Figure 12.- Absolute statistical uncertainty ratio for the V-component of velocity.

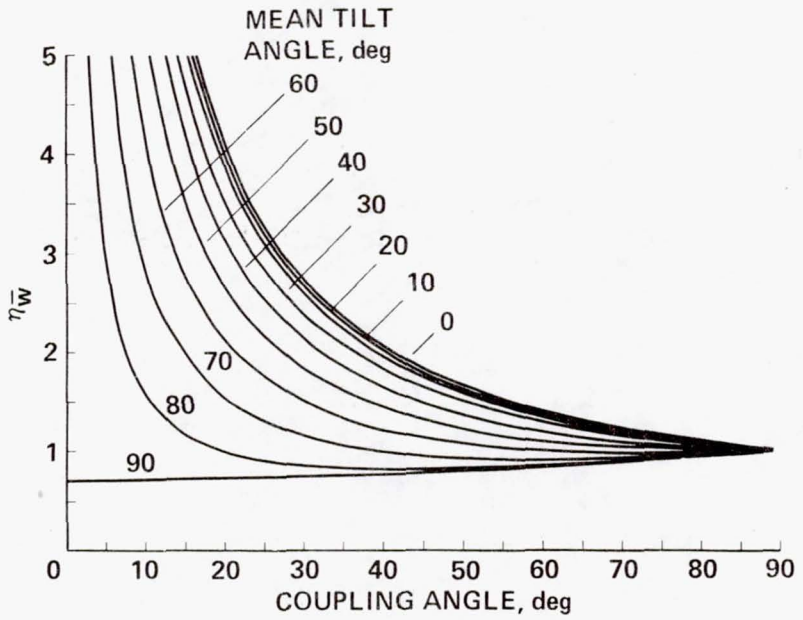

Figure 13.- Absolute statistical uncertainty ratio for the W-component of velocity.

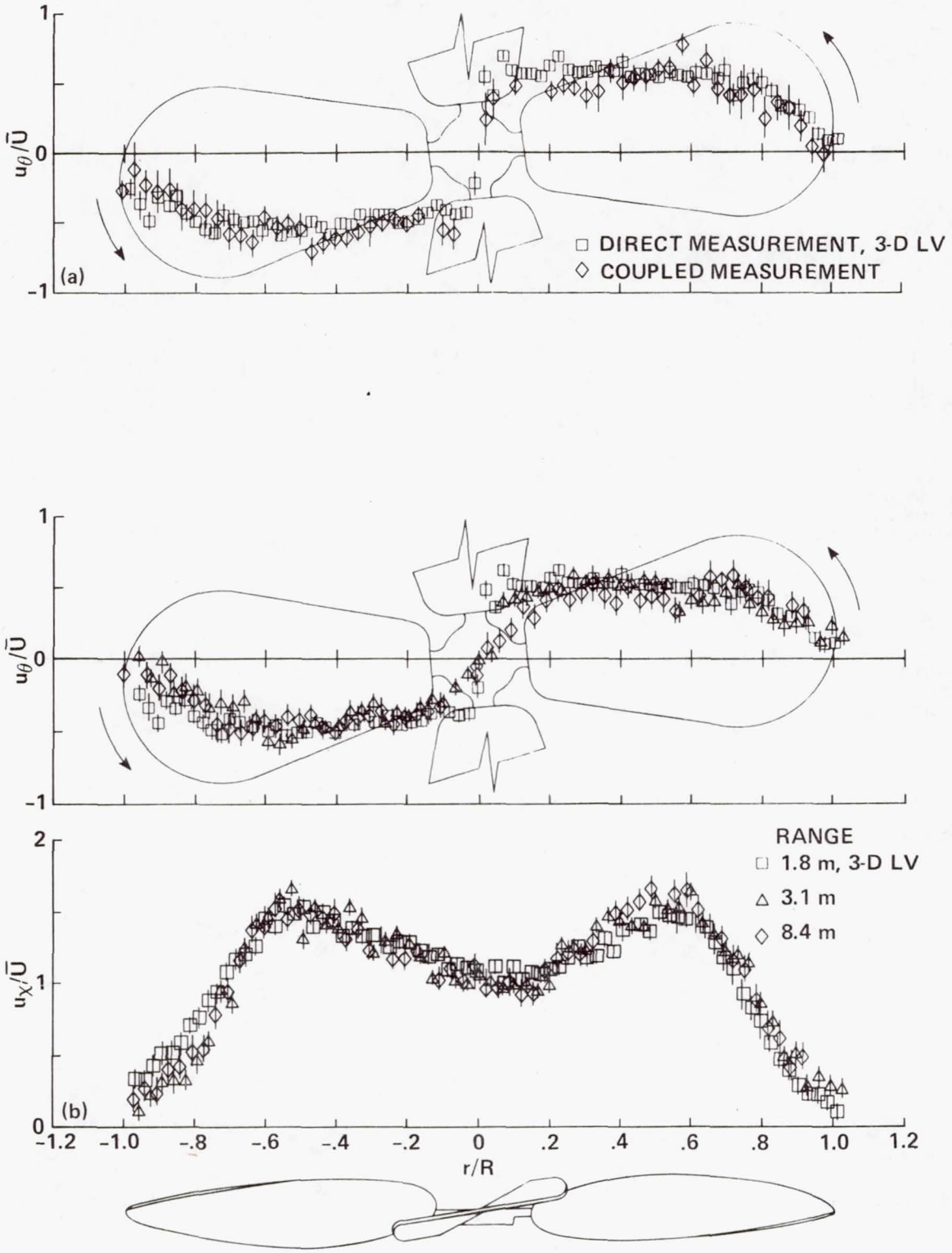

Figure 14.- Nondimensionalized velocity surveys across a fan comparing direct short-range measurements taken with the two-dimensional portion of a three-dimensional LV with: (a) the profile determined from coupled long-range measurements; (b) profiles measured directly at long range.

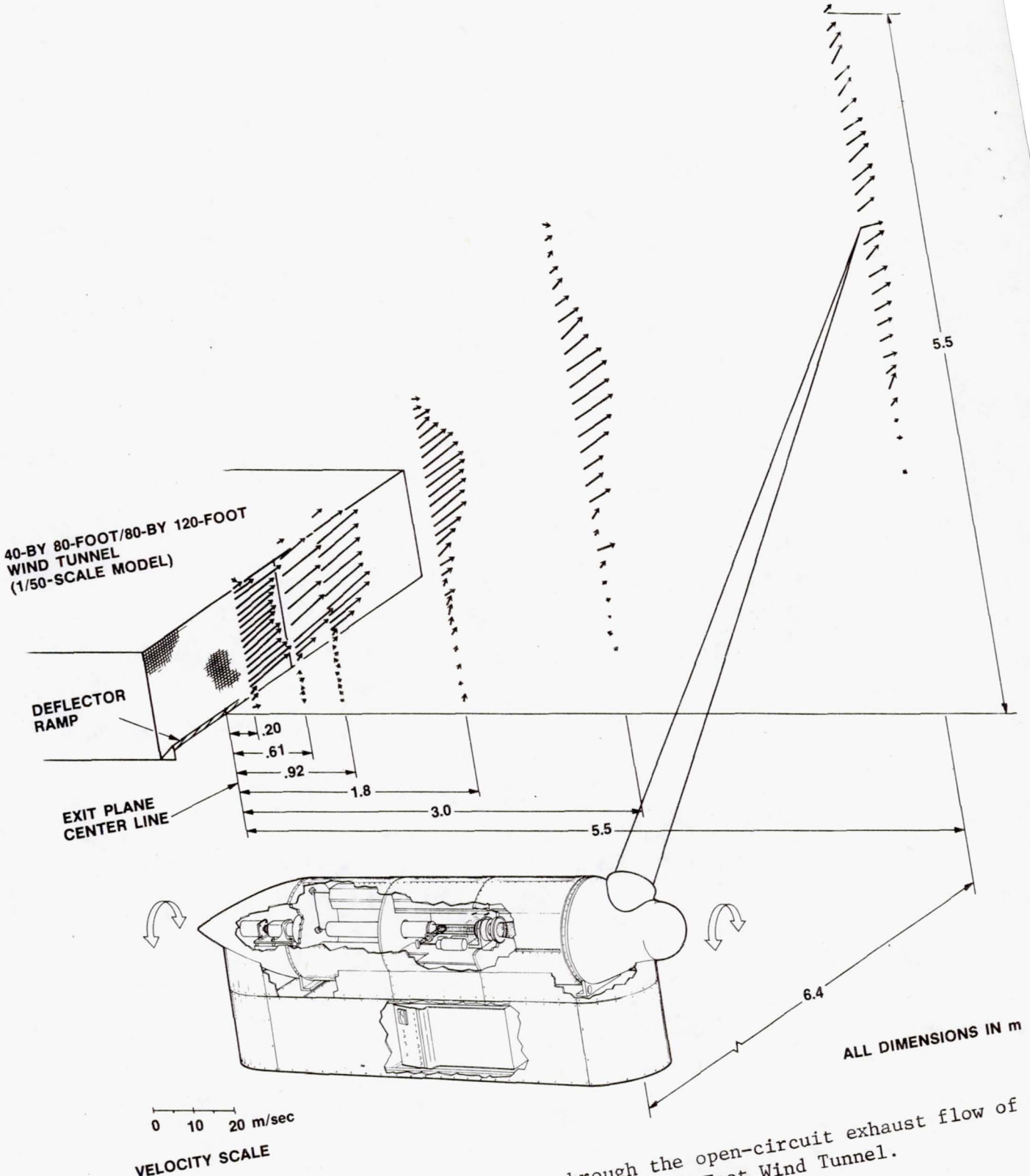

Figure 15.- Vertical velocity surveys through the open-circuit exhaust flow of the 1/50-scale model of the 80- by 120-Foot Wind Tunnel.

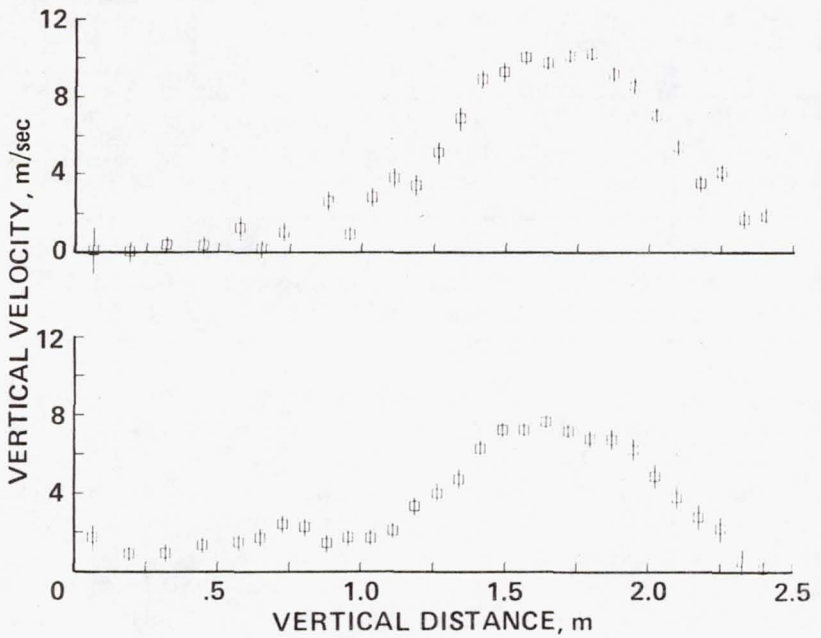

Figure 16.- Vertical velocity survey taken at 1.8 m from the wind-tunnel exit plane showing the vertical and horizontal velocity components.

1. Report No.	2. Government Accession No.	3. Recipient's Catalog No.
NASA TM-84393		

4. Title and Subtitle	5. Report Date
A LASER VELOCIMETER SYSTEM FOR LARGE-SCALE AERODYNAMIC TESTING	November 1983
	6. Performing Organization Code

7. Author(s)	8. Performing Organization Report No.
Michael S. Reinath, Kenneth L. Orloff, and Philip K. Snyder	A-9524
	10. Work Unit No. T3839YA

9. Performing Organization Name and Address	11. Contract or Grant No.
Ames Research Center Moffett Field, California 94035	
	13. Type of Report and Period Covered
12. Sponsoring Agency Name and Address	Technical Memorandum
National Aeronautics and Space Administration Washington, D.C. 20546	14. Sponsoring Agency Code 505-31-51

15. Supplementary Notes

Point of Contact: Michael S. Reinath, Ames Research Center, M/S 247-1, Moffett Field, Calif. 94035 (415) 965-6680 or FTS 448-6680.

16. Abstract

A unique laser velocimeter has been developed that is capable of sensing two orthogonal velocity components from a variable remote distance of 2.6 to 10 m for use in the 40- by 80-Foot and 80- by 120-Foot Wind Tunnels and the Outdoor Aerodynamic Research Facility at Ames Research Center. The system hardware, positioning instrumentation, and data acquisition equipment are described in detail; system capabilities and limitations are discussed; and expressions for systematic and statistical accuracy are developed. Direct and coupled laboratory measurements taken with the system are compared with measurements taken with a laser velocimeter of higher spatial resolution, and sample data taken in the open circuit exhaust flow of a 1/50-scale model of the 80- by 120-Foot Wind Tunnel are presented.

17. Key Words (Suggested by Author(s))	18. Distribution Statement
Long-range laser velocimetry	Unlimited Subject Category - 02

19. Security Classif. (of this report)	20. Security Classif. (of this page)	21. No. of Pages	22. Price*
Unclassified	Unclassified	31	A03

*For sale by the National Technical Information Service, Springfield, Virginia 22161